ADVANCES IN ATMOSPHERIC SCIENCES, VOL. 32, OCTOBER 2015, 1381–1390

A Comparative Study on the Dominant Factors Responsible for the Weaker-than-expected El Niño Event in 2014

LI Jianying[1,3], LIU Boqi[1,4], LI Jiandong[1], and MAO Jiangyu*[1,2]

[1]*State Key Laboratory of Numerical Modeling for Atmospheric Sciences and Geophysical Fluid Dynamics, Institute of Atmospheric Physics, Chinese Academy of Sciences, Beijing* 100029

[2]*Joint Center for Global Change Studies, Beijing* 100875

[3]*University of Chinese Academy of Sciences, Beijing* 100049

[4]*Chinese Academy of Meteorological Sciences, Beijing* 100081

(Received 8 December 2014; revised 9 April 2015; accepted 6 May 2015)

ABSTRACT

Anomalous warming occurred in the equatorial central-eastern Pacific in early May 2014, attracting much attention to the possible occurrence of an extreme El Niño event that year because of its similarity to the situation in early 1997. However, the subsequent variation in sea surface temperature anomalies (SSTAs) during summer 2014 in the tropical Pacific was evidently different to that in 1997, but somewhat similar to the situation of the 1990 aborted El Niño event. Based on NCEP (National Centers for Environmental Prediction) oceanic and atmospheric reanalysis data, the physical processes responsible for the strength of El Niño events are examined by comparing the dominant factors in 2014 in terms of the preceding instability of the coupled ocean–atmosphere system and westerly wind bursts (WWBs) with those in 1997 and 1990, separately. Although the unstable ocean–atmosphere system formed over the tropical Pacific in the preceding winter of 2014, the strength of the preceding instability was relatively weak. Weak oceanic eastward-propagating downwelling Kelvin waves were forced by the weak WWBs over the equatorial western Pacific in March 2014, as in February 1990. The consequent positive upper-oceanic heat content anomalies in the spring of 2014 induced only weak positive SSTAs in the central-eastern Pacific–unfavorable for the subsequent generation of summertime WWB sequences. Moreover, the equatorial western Pacific was not cooled, indicating the absence of positive Bjerknes feedback in early summer 2014. Therefore, the development of El Niño was suspended in summer 2014.

Key words: El Niño event, westerly wind burst, instability of coupled ocean–atmosphere system, positive Bjerknes feedback

Citation: Li, J. Y., B. Q. Liu, J. D. Li, and J. Y. Mao, 2015: A comparative study on the dominant factors responsible for the weaker-than-expected El Niño event in 2014. *Adv. Atmos. Sci.*, **32**(10), 1381–1390, doi: 10.1007/s00376-015-4269-6.

1. Introduction

It is well known that El Niño refers to anomalous warm episodes during which sea surface temperatures (SSTs) in the central and eastern tropical Pacific are warmer than normal (Philander, 1985). El Niño is also considered as the warm phase of the El Niño–Southern Oscillation (ENSO) cycle in the coupled atmosphere–ocean system. As a dominant variability in the air–sea interacting system on the interannual timescale, ENSO significantly affects the tropical and extratropical climate (Yang, 1996; Webster et al., 1998; Wang, 2000; Wang, 2000; Mao and Wu, 2007; Sun and Yang, 2007; Zheng et al., 2009). Therefore, it is of great importance to monitor and forecast the evolution of ENSO events.

In early May 2014, anomalous warming was observed in the equatorial central-eastern Pacific (National Aeronautics and Space Administration, 2014) digital dash, and the pattern and magnitude of satellite-based sea surface height anomalies (SSHAs) bore a close resemblance to those in May 1997. Since the 1997–98 El Niño was the strongest warm episode among the ENSO cycles in the 20th century, the similar SSHAs and predictions derived from some climate models (Tollefson, 2014) suggested that a super El Niño event would possibly develop during subsequent months in 2014. However, the warming remained in an unexpectedly neutral state at the end of August 2014 (Australian Government Bureau of Meteorology, 2014), rather different from the situation in August 1997 when a mature El Niño had already occurred. Although the latest climate model results predicted that the 2014 El Niño would subsequently resurge (Zastrow, 2014), it is still unclear as to why the equatorial central-eastern Pacific warming suspended that summer. Actually, the strength of an El Niño event depends mainly on two dominant factors: the preceding instability of the tropical Pacific ocean–atmosphere coupled system (Wyrtki, 1975, 1985; Jin, 1997;

* Corresponding author: MAO Jiangyu
Email: mjy@lasg.iap.ac.cn

Fedorov et al., 2015; Lai et al., 2015) and the westerly wind bursts (WWBs) over the equatorial western-central Pacific.

Before the onset of El Niño, warm water masses accumulate in the equatorial western Pacific [EWP; (5°S–5°N, 130°–170°E)], forming a stronger equatorial zonal SST contrast and a steeper tilting of the thermocline through the dynamical thermostat mechanism (Clement et al., 1996; Sun and Liu, 1996). Thus, the ocean–atmosphere coupled system over the tropical Pacific becomes unstable. El Niño events act as a major mechanism to transport the accumulated warm water poleward and eastward, so as to recover a stable state (Sun, 2003).

When the preceding unstable ocean–atmosphere coupled system is formed, the equatorial WWBs could trigger an El Niño event. Many studies have suggested that the occurrence of equatorial WWBs are closely associated with the Madden–Julian Oscillation (MJO; Madden and Julian, 1971, 1972). The MJO is an intraseasonal coupled convection-circulation system (Hendon and Salby, 1996). When the wet phase of MJO moves eastward into the western Pacific, a strong westerly anomaly (namely, a WWB) following the deep convection can force an oceanic downwelling Kelvin wave along the thermocline (Hendon and Glick, 1997). The deepened thermocline causes positive SSTAs in the equatorial central-eastern Pacific, thus triggering an El Niño event (Lau and Chan, 1986; Kiladis et al., 1994; McPhaden, 1999; Fasullo and Webster, 2000; Zhang and Gottschalck, 2002). Therefore, the strength of El Niño events depends largely on the magnitudes of the preceding instability and WWBs.

Although the positive SSHAs in early 2014 exhibited some similarities to those in early 1997, the evolution of the oceanic Niño3.4 index (ONI) after May 2014 became different from that in 1997. Instead, the SSTA pattern in May–August 2014 was analogous with its 1990 counterpart. The mean pattern correlation coefficient (Taylor, 2001) of the monthly SSTAs in the Niño3.4 region (5°S–5°N, 120°–170°W) for the period May–August between 2014 and 1990 is 0.75, which is the largest among the coefficients from 1982 to 2013. Therefore, it is necessary to investigate how the super El Niño-like initial ocean state in early 2014 evolved subsequently into SSTA patterns similar to an aborted El Niño in 1990 in summertime.

Recently, Menkes et al. (2014) argued that, due to the lack of WWB sequences in April–July 2014, no oceanic downwelling Kelvin waves were observed, and then the eastern edge of the warm pool also retreated to its climatological position. Thus, the anomalous warming was restrained in summer 2014. Moreover, Vecchi and Harrison (2000) and Lengaigne et al. (2003) suggested that the location of the warm pool could also influence the occurrence of WWBs, implying a positive feedback process between positive SSTAs and WWBs. Since Menkes et al. (2014) only focused on the dynamical forcing of WWBs on the oceans, and since the warm SSTAs in the equatorial central-eastern Pacific are also related to the preceding instability of the ocean–atmosphere coupled system (Sun, 2003; Fedorov et al., 2015; Lai et al., 2015), the objective of this paper is to reveal the mechanism responsible for the SSTA evolution in the tropical Pacific related to the 2014 El Niño event. We approach this by comparing the WWBs and the preceding instability of the ocean–atmosphere coupled system in 2014 with those in 1997 and 1990. In doing so, we hope to better understand why the predicted strong El Niño event in 2014 decayed in the summer, as well as the key physical processes responsible for the strength of El Niño events in general.

2. Data and methods

The ONI and Southern Oscillation index (SOI) provided by National Oceanic and Atmospheric Administration (NOAA) Climate Prediction Center (CPC) are used to detect the ENSO state. The ONI is defined as a three-month running mean of area-averaged SSTAs in the Niño3.4 region, and the SOI is calculated as the difference of standardized sea level pressure anomalies between the stations of Tahiti and Darwin. Daily SSTs are derived from the NOAA Optimum Interpolation 1/4 Degree Daily Sea Surface Temperature (OISST) analysis (Reynolds et al., 2007) with a horizontal resolution of $0.25^\circ \times 0.25^\circ$. To depict the ENSO-related oceanic dynamics, pentadly gridded oceanic temperature obtained from the National Centers for Environmental Prediction (NCEP) Global Ocean Data Assimilation System (GODAS) (Behringer and Xue, 2004) are employed to calculate the oceanic heat content of the upper ocean (0–300 m) (Xue et al., 2012) and to diagnose the heat budget in the mixed layer. These oceanic reanalysis data have a horizontal resolution of $1^\circ \times 0.33^\circ$ and 40 levels in the vertical direction, with a 10 m resolution in the upper 200 m. In the atmosphere, the daily surface zonal winds are derived from the NCEP/National Center for Atmospheric Research (NCAR) reanalysis (Kalnay et al., 1996) with a horizontal resolution of $2.5^\circ \times 2.5^\circ$. Both the oceanic temperature and surface wind data cover the period from 1 January 1981 to 31 August 2014.

Toyoda et al. (2009) suggested that the persistently high SST condition over the equatorial central Pacific [ECP; (5°S–5°N, 160°E–160°W)] favors the generation of an unstable coupled wave, which is an important feature of strong El Niño events. As the SST behavior can be well represented by the mean temperature in the mixed layer (Sun et al., 2014), the oceanic mixed layer heat budget is diagnosed to examine the contribution of air–sea heat flux and oceanic processes to the SST variations in 2014. The heat budget of the mixed layer is written as

$$\frac{\partial T'}{\partial t} = (-\boldsymbol{V}\cdot\nabla T)' + \left(-w\frac{\partial T}{\partial z}\right)' + \left(\frac{Q_{\text{net}}}{\rho c_p H}\right)' + R, \quad (1)$$

where a prime represents the anomaly from the 1981–2010 climatology, T' represents the anomalous temperature averaged in the mixed layer, $\boldsymbol{V}$ denotes the horizontal ocean current, w is the oceanic vertical motion, Q_{net} represents net heat flux at the oceanic surface, ρ is the constant oceanic density (10^3 kg m^{-3}), $c_p = 4000$ J kg^{-1} K^{-1} denotes the specific heat of water, and H represents the mixed layer depth. The

first three terms on the right-hand side of Eq. (1) represent the anomalous advection, entrainment and net air–sea heat flux, respectively, whereas R is the residual term.

3. Comparison of the dominant factors associated with El Niño strength among 1989–90, 1996–97 and 2013–14

Table 1 presents the time series of ONI from December 2013 to August 2014. It also shows the situation in 1990 and 1997 for comparison. In 1997, the ONI changed from negative to positive in spring (March–May), and intensified rapidly in late spring, with the ONI reaching 0.7°C to satisfy the onset criterion (exceeding the threshold of 0.5°C) of an El Niño event. Subsequently, the ONI strengthened continually in the following months, and the El Niño event already became a strong event in the summer. In 2014, the ONI increased evidently from −0.5°C to −0.1°C from March to April (Table 1), and then turned to positive in the early summer (April–June), exhibiting a similar situation to that in 1997. However, the ONI remained at 0.1°C in mid-summer (May–July) and even dropped to zero in June–August, rather than rapidly increasing as it did in the summer of 1997. This decay from an El Niño-favored condition in spring to a neutral state in summer indicates that the warming in the equatorial central-eastern Pacific was suspended in summer, as was the case in 1990. Although the ONI had already become positive and increased gradually in the spring of 1990, it also remained unchanged from April to July. Eventually, such an El Niño-like event was aborted in late 1990. In order to quantitatively examine to what extent the 2014 El Niño resembled the 1990 case during the summer, we calculated the pattern correlations between 2014 and each of the other years. Indeed, the largest mean (May–August) correlation coefficient appeared in 1990, indicating that the El Niño evolution in May–August 2014 most closely resembled that in 1990.

Given that the strength of El Niño events depends largely on the preceding instability of the tropical Pacific ocean–atmosphere coupled system and equatorial WWBs (Lau and Chan, 1986; Kiladis et al., 1994; McPhaden, 1999; Fasullo and Webster, 2000; Zhang and Gottschalck, 2002; Sun, 2003), we compared these dominant factors during their pre-developing and developing phases (from the previous winter to the current summer) to understand why the development of anomalous warming in the equatorial central-eastern Pacific suspended in the summer of 2014 (Zastrow, 2014).

3.1. *Evolution of the dominant factors from the previous winter to the current spring of El Niño events*

3.1.1. *Preceding instability of the tropical Pacific air–sea coupled system*

The heat pump hypothesis proposed by Sun (2003) suggests that the preceding instability of the ocean–atmosphere coupled system over the tropical Pacific is an important factor in determining the strength of an El Niño event. Figure 1 shows the time series of standardized upper oceanic heat content (UOHC) anomalies in the EWP and equatorial eastern Pacific [EEP; (5°S–5°N, 90°–140°W)]. Significant positive UOHC anomalies existed in the EWP, while the negative UOHC anomalies in the EEP were different in terms of their magnitude and duration from the previous November to the current February in each individual year (Fig. 1). The sustained positive UOHC anomalies in the EWP and the undulating negative UOHC anomalies in the EEP led to a

Table 1. Time series of the oceanic Niño3.4 index (ONI) (°C) in 1990, 1997, and 2014. See text in section 2 for the definition of the ONI.

Year	DJF	JFM	FMA	MAM	AMJ	MJJ	JJA
1990	0.1	0.2	0.3	0.3	0.2	0.2	0.3
1997	−0.5	−0.4	−0.1	0.2	0.7	1.2	1.5
2014	−0.6	−0.6	−0.5	−0.1	0.1	0.1	0.0

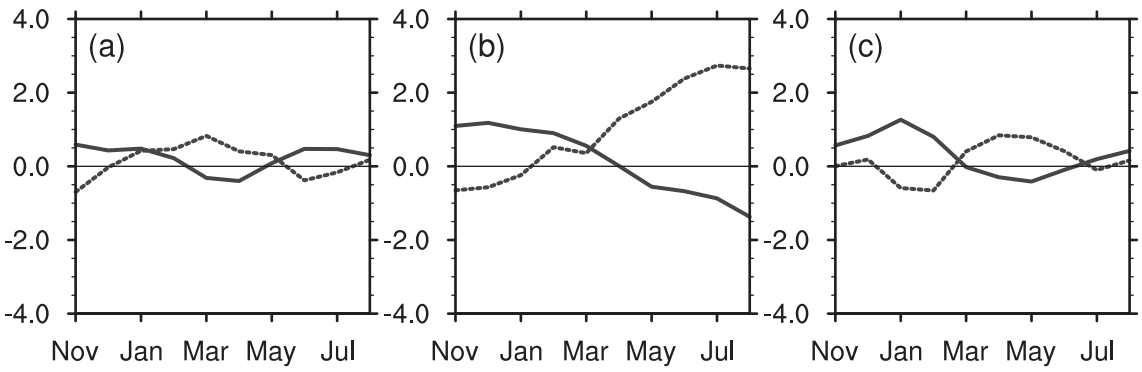

Fig. 1. Time series of area-averaged standardized UOHC anomalies over the EWP (5°S–5°N, 130°–170°E) (solid line) and over the EEP (5°S–5°N, 90°–140°W) (dashed line) for the periods of (a) 1 November 1989 to 31 August 1990, (b) 1 November 1996 to 31 August 1997, and (c) 1 November 2013 to 31 August 2014.

steeper tilting of the thermocline in the entire Pacific in all the three years, which indicates the presence of an unstable air–sea coupled system over the tropical Pacific. Such ocean states in the previous winter supported the occurrence of an El Niño event for all three cases.

Note that the preceding instability in winter 1989 and 2014 were smaller compared with that in 1997, implying that the magnitudes of the potential equatorial central-eastern Pacific warming in the subsequent months would be smaller.

3.1.2. *WWBs from the previous winter to the current spring of El Niño events*

Figure 2 displays the evolution of the surface zonal winds and equatorial UOHC anomalies before and during the El Niño developing phases in the three years. Strong surface westerly winds (a WWB) were observed over the equatorial western-central Pacific in early December 1989, late December 1996 and mid-January 2014 (Figs. 2a–c). Note that the patterns and variation of the observed surface zonal winds were in agreement with its intraseasonal (30–60-day filtered) anomalies over the EWP, indicating the dominant role of the MJO in generating these WWBs. The WWBs over the equatorial western-central Pacific could produce eastward propagating positive UOHC anomalies (e.g., McPhaden, 1999) by inducing an oceanic downwelling Kelvin wave (indicated by the solid line) to deepen the thermocline in the ECP, as suggested by Lengaigne et al. (2003). As a result, positive UOHC anomalies were observed in the ECP around mid-December 1989 (Fig. 2d), mid-January 1996 (Fig. 2e) and February 2014 (Fig. 2f).

Note that the warming in the upper ocean of the ECP from December 1989 to January 1990 and January–February 2014 was weaker than that in January–February 1997 (Figs. 2d–f). The high SST condition in the ECP during the preceding winter of an El Niño event could influence the intensity of WWBs over the EWP in the subsequent spring (Bergman et al., 2001; Chiodi et al., 2014). It is conceivable that the warmer ECP in the winter of 1996–1997 facilitated a stronger WWB in the spring of 1997. In order to quantitatively measure the strength of WWBs, a westerly wind index (WWI) was defined as standardized surface zonal wind anomalies, area-averaged over the EWP. As expected, a strong WWB in March 1997 (Fig. 2b), with a WWI greater than 1.0, was observed, while a moderate WWB in March 2014 (Fig. 2c) and a weak WWB appeared in February 1990 (Fig. 2a), with WWIs both less than 0.5 (Table 2).

As a response to the strong WWB in early March 1997, the positive anomalous UOHC had aggressively developed to substantially deepen the thermocline over the ECP from mid-March onwards. Through thermocline-associated anomalous entrainments and WWB-related anomalous zonal advection, the ECP was greatly warmed in April (Fig. 3b and 4b). As suggested by Toyoda et al. (2009), high SST in the ECP could excite intense air–sea interaction, which was manifested as a positive feedback between anomalous surface westerlies and positive SSTAs. Firstly, the positive SSTAs in the ECP decreased the zonal gradient of SST in the tropical Pacific, thus causing the anomalous surface westerly. Afterwards, the forced anomalous surface westerly transported more warm water to the ECP via the anomalous westerly wind stress (not shown), and thus the positive SSTAs over the ECP were substantially strengthened. Such an intense air–sea interaction further triggered a large-amplitude unstable air–sea coupled wave, propagating eastward at a slower speed of 0.5 m s^{-1} (indicated by the dashed line in Fig. 2b), which was slower than the oceanic Kelvin waves with a speed in the range of 2–2.5 m s^{-1} (the solid lines in Fig. 2). The positive UOHC anomaly reached the EEP in early May and warmed the SST rapidly, characterized by the ONI reaching 0.7 in April–June (Table 1). Meanwhile, the EWP was cooled through the wind–evaporation–SST (Xie et al., 1993; Cronin and McPhaden, 1997; Hendon and Glick, 1997) and the cloud–radiation–SST feedback (Lau and Sui, 1997; Jones et al., 1998). Therefore, a zonal dipole SSTA pattern was established over the equatorial Pacific in April–May 1997 (Fig. 4b). In response to this SSTA pattern, the zonal gradient of sea level pressure decreased, with the SOI dropping from 0.2 to −1.1 in March–May (Table 3). The consequently weakened easterly trade winds in a negative Southern Oscillation phase in turn strengthened the EEP warming through thermocline feedback, thus establishing a positive Bjerknes feedback (Bjerknes, 1969).

Table 2. Time series of the standardized westerly wind index (WWI) in 1990, 1997, and 2014. See text in section 3.1.2 for the definition of the WWI.

Year	DJF	JFM	FMA	MAM	AMJ	MJJ	JJA
1990	0.3	0.5	0.1	−0.4	−1.0	−1.0	−1.0
1997	0.1	1.1	1.2	1.4	0.5	0.1	0.2
2014	0.5	0.3	0.3	−0.6	−1.2	−1.5	−1.3

Table 3. Time series of the three-month running mean Southern Oscillation index (SOI) in 1990, 1997, and 2014. See text in section 2 for the definition of the SOI.

Year	DJF	JFM	FMA	MAM	AMJ	MJJ	JJA
1990	−1.2	−0.8	−0.7	0.3	0.6	0.7	0.2
1997	1.3	0.6	0.2	−0.8	−1.1	−1.2	−1.2
2014	0.5	0.2	0.0	0.1	0.5	0.2	−0.2

For the case in 1990, because of the relatively weak WWB in February (Fig. 2a), the resultant thermocline-related anomalous entrainment and zonal advection led to a weak positive SSTA tendency in the ECP in February (Fig. 3a). Subsequently, the anomalous entrainment decayed substantially while the sign of the advection term turned negative, resulting in a negative SSTA tendency in March. Therefore, the following warming in the ECP was so weak that the positive SSTAs were limited to a very local area in April (Fig. 4a). The weak SST warming was unfavorable for the formation of positive feedback between the anomalous surface westerly and positive SSTAs over the ECP, and thus no unstable coupled waves were generated (Fig. 2d). Therefore, the positive UOHC anomalies still propagated eastward in the manner of an independent oceanic Kelvin wave. In contrast to the 1997 spring, the upper ocean warming weakened but propagated eastward at a speed of 2.55 m s^{-1} from mid-February to mid-April in 1990 (Fig. 2d). The consequent surface warming over the EEP in early May was also much weaker, manifesting as the ONI decreased slightly from March–May to April–June (Table 1). The oceanic cooling in the EWP was also weaker in March–April 1990 and almost disappeared in May (Fig. 4a). In response to this SSTA pattern, the SOI turned positive in April (Table 3), indicating that no positive Bjerknes feedback was established in spring 1990.

Although the WWB in March 2014 was stronger than that in February 1990 (Figs. 2a and c; Table 2), the succeeding evolution of UOHC anomalies in March–May 2014 resembled the counterpart from February to mid-April in 1990. Specifically, the positive UOHC anomalies propagated eastward at a constant speed from March to May without strengthening, which indicates that the unstable ocean–atmosphere coupled wave also failed to establish. According to the results of mixed layer heat budget analysis (Fig. 3c), the co-effect of oceanic horizontal advection and entrainment similarly warmed the ECP in March 2014. However, as the WWB in spring 2014 was much weaker than that in March 1997 (Figs. 2b and c; Table 2), the warming speed of the SST over the ECP in March 2014 was much slower than that in March 1997 (Figs. 4b and c). The entrainment then weakened substantially in April, and the advection in the mixed layer began to cool the ECP SST (Fig. 3c). Consequently, the ECP was not warm enough to support the development of positive feedback between SSTAs and surface westerly anomalies. As a result, no WWB occurred after April, and there was no westerly wind stress (not shown) to further trigger the oceanic downwelling Kelvin wave. Since the air–sea interaction in the spring of 2014 was suppressed, only the oceanic downwelling Kelvin wave induced by the WWB reached the EEP in May 2014, leading to a moderate surface warming with the ONI turning positive (Table 1). Note that the EWP was not cooled as expected. Similar to the situation in spring 1990, the zonal gradient of sea level pressure decreased slightly, and thus the SOI also remained positive in spring 2014 (Table 3), implying the absence of positive Bjerknes feedback.

3.2. *Evolution of the dominant factors during the current summer of El Niño events*

3.2.1. *WWBs during the current summer of El Niño events*

As the positive Bjerknes feedback between SST and zonal wind anomalies (Bjerknes, 1969) had already established in spring 1997, the SOI remained negative in summer. In response to the decreased zonal gradient of sea level pressure, easterly trade winds were further weakened—favorable for WWBs to occur more frequently in summertime (Fig. 2b). In contrast, the positive Bjerknes feedback failed to establish in the summer of 1990, the SOI remained positive, and ONI increased slowly. In this situation, the anomalous westerlies were too weak to overcome the climate-mean easterly trade winds over the EWP (Fig. 2a), with the WWI being negative in June–August 1990 (Table 2). In June–July 2014, although prominent positive SSTAs were present in the EEP, the EWP was not controlled by negative SSTAs as expected (Fig. 4c). As a result, the SSTA in the equatorial Pacific was characterized by a monopole pattern, which was rather similar to the situation in May 1990. Since positive Bjerknes feedback was absent even in the early summer of 2014, it is reasonable to deduce that no strong WWBs over the EWP would be induced in the summer of 2014 (Fig. 2c and Table 2).

Furthermore, the evolution of WWBs is closely associated with the eastward extension of the warm pool in the equatorial Pacific. Previous studies (Bergman et al., 2001; Lengaigne et al., 2003) have suggested that the eastward displacement of the warm pool in turn promotes deep convection further into the ECP. Here, we investigated the feedback between the eastward expanding warm pool and the MJO-related WWBs. The amplitude of the MJO-related WWBs at a particular time t is defined as the standardized deviation of the 30–60-day filtered surface zonal winds for a 61-day period ranging from $t-30$ to $t+30$ days. In April–August 1997, the ECP was substantially warmed due to the WWB-induced eastward propagating unstable air–sea coupled wave. Thus, the warm pool extended significantly, represented by the eastward displacement of the 29°C isotherm to around 150°W (Fig. 4b). Before May 1997, the MJO-related WWBs were confined to the west of the dateline (Fig. 4e). Evident MJO-related WWBs appeared to the east of the dateline in June 1997, suggesting that the eastward extension of the warm pool had indeed strengthened the convective activities and WWBs over the ECP. As the WWBs extended eastward to around 140°W from May to June (Fig. 2b), the positive UOHC anomalies were further enhanced in the ECP through positive feedback between SSTAs and WWBs.

From spring to summer in 1990 and 2014, the sea surface warming in the ECP was much weaker than that in 1997, with the eastern edge of warm pool settling around the dateline (Figs. 4a and c). Although the eastern edge had shifted temporarily to the east of the dateline in early May 2014, in mid-June it retreated quickly back to the dateline—its climatological position. Since the SST condition over the ECP was inadequately warm, the zonal SSTA gradient and gradient of

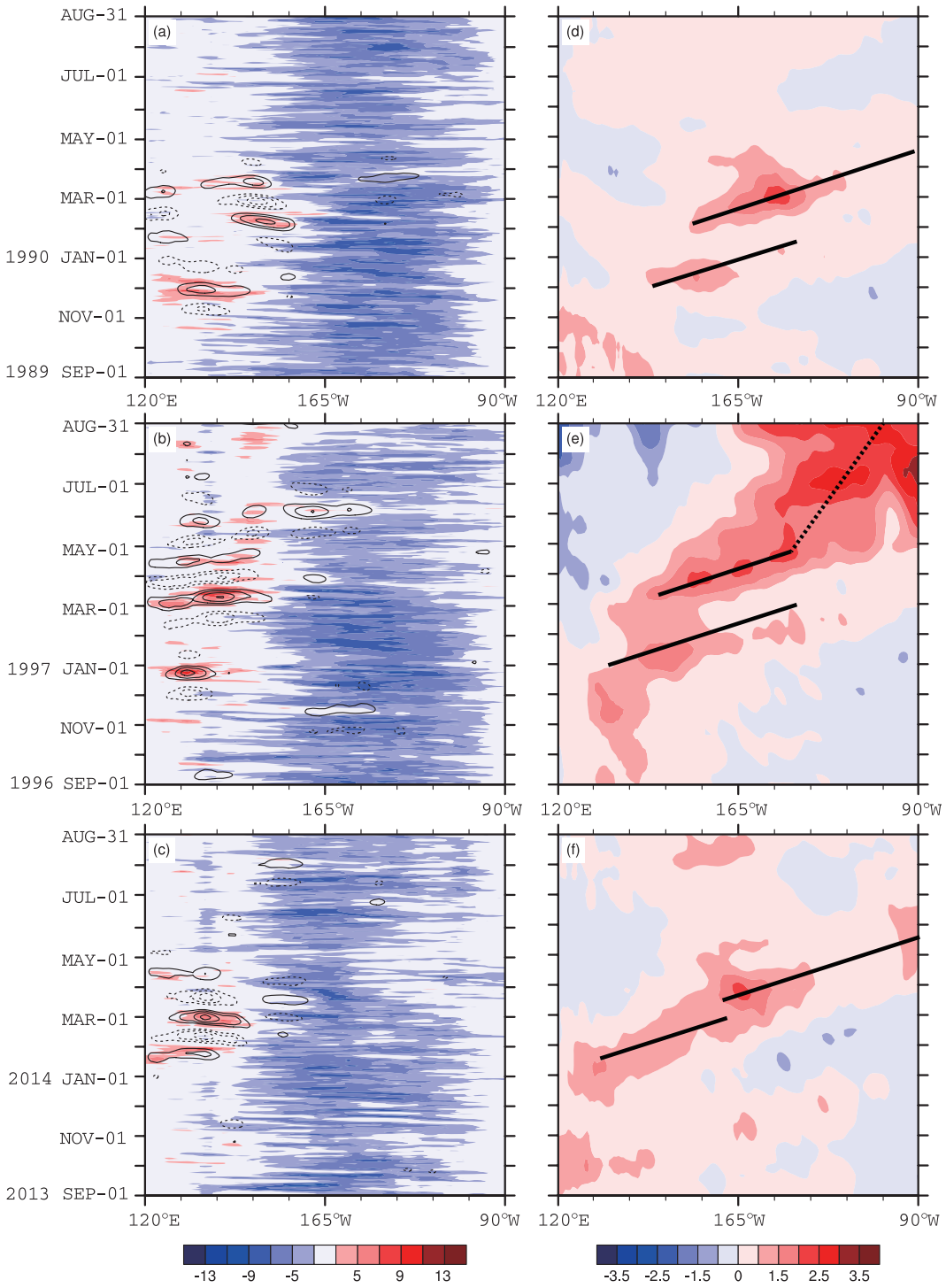

Fig. 2. Time–longitude cross sections of equatorial (5°S–5°N) surface zonal winds (color scale, m s^{-1}) and 30–60-day filtered zonal wind anomalies (contours, m s^{-1}) for the periods of (a) 1 September 1989 to 31 August 1990, (b) 1 September 1996 to 31 August 1997, and (c) 1 September 2013 to 31 August 2014. Positive and negative anomalies are shown as solid and dashed contours, respectively; the zero-contours are omitted; the contours start from 1.0, with an interval of 0.5. (d–f) As in (a–c) but for UOHC anomalies (color scale, K). Solid lines indicate the propagation of the oceanic downwelling Kelvin wave. The dashed line denotes the propagation of the unstable air–sea coupled wave.

sea level pressure anomalies between the EWP and ECP were very weak. Thus, no evident WWB was observed from late April to August in 1990 and 2014 (Figs. 4d and f). Considering the absence of WWB sequences, the development of the EEP warming was suspended, and thus the ONI in summer 1990 failed to meet the El Niño criterion and the expected 2014 El Niño decayed to a neutral state in summer, consistent with the findings of Menkes et al. (2014).

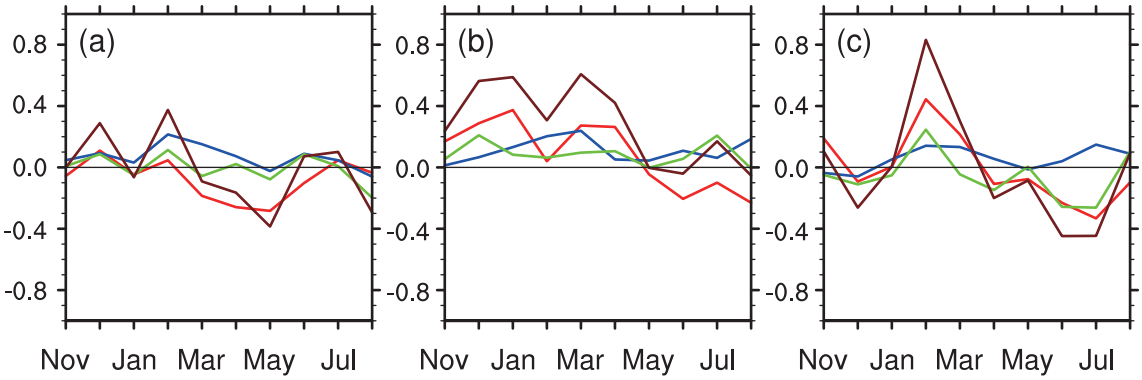

Fig. 3. Time series of the three-month running mean mixed layer anomalous horizontal advection term (red line, K month^{-1}), entrainment term (blue line, K month^{-1}) and net surface heat flux term (green line, K month^{-1}), area-averaged over the ECP (5°S–5°N, 160°E–160°W) for the periods of (a) 1 November 1989 to 31 August 1990, (b) 1 November 1996 to 31 August 1997, and (c) 1 November 2013 to 31 August 2014. Also shown is the sum of these three terms (brown line, K month^{-1}).

3.2.2. *The tropical Pacific air–sea coupled system during the current summer of El Niño events*

The intense unstable ocean–atmosphere coupled waves induced by the strong WWB in March 1997 (Fig. 2c) could transport warm water eastward to warm the EEP substantially, causing positive SSTAs in the eastern Pacific (Figs. 2e and 4b). The positive SSTAs in turn forced off-equatorial cyclonic wind stress anomalies to the west on both sides of the equator (Matsumo, 1966; Gill, 1980). The cyclonic wind stress anomalies enhanced poleward heat transport, and then cooled the EWP dramatically (Fig. 1b). As a result, the positive UOHC anomalies in the EWP disappeared and the coupled air–sea system was stabilized in May 1997. Since the positive Bjerknes feedback had already established at this time, the western cooling and eastern warming developed continually, ultimately causing the super El Niño in the fall–winter of 1997.

For 1990 and 2014, although the EEP warming and associated poleward heat transport were weaker, the unstable coupled system was still stabilized in May 1990 and June 2014 (Figs. 1a and c). As the positive Bjerknes feedback failed to establish in the spring of 1990 and 2014, the EEP warming was suspended in June–August 1990 and mid-July 2014 (Figs. 4a and c).

Positive UOHC anomalies were again observed in the EWP in June 1990 and July 2014, indicating the rebirth of the unstable coupled system. However, since fall is usually a rapidly developing period for El Niño events, there was not enough time left for the re-accumulation of sufficient energy to form a strong El Niño event in late 2014. Thus, the predicted super El Niño event did not take place in the boreal winter of 2014.

4. Summary and discussion

In order to clarify why the warming in the equatorial central-eastern Pacific was suspended in summer 2014, a comparative analysis was conducted to demonstrate the similarities and differences between the El Niño event in that year with its counterparts in 1990 and 1997. The dominant factors responsible for the strength of El Niño events were compared in terms of the WWBs and preceding instability of the tropical Pacific ocean–atmosphere coupled system.

A strong unstable state of the coupled ocean–atmosphere system over the tropical Pacific was formed during the previous fall and winter in 1997, indicating its initial oceanic state was favorable for the development of a strong El Niño event in the following year. This accumulated instability was then released by the WWB in spring 1997 and triggered a strong El Niño event. The strong WWB in March 1997 led to prominent warming over the ECP by triggering strong oceanic downwelling Kelvin waves and through oceanic zonal advection feedback. The strongly warmed ECP provided a favorable stage for the development of air–sea interaction, thus generating an eastward propagating unstable air–sea coupled wave, which further warmed the equatorial central-eastern Pacific. Since the WWB in spring 1997 also cooled the EWP, the decreased zonal SST gradient along the equator led to a negative phase of Southern Oscillation in spring, which in turn strengthened the EEP warming through thermocline feedback. Since such a positive Bjerknes feedback had established in spring 1997, the warming over the equatorial central-eastern Pacific continued to develop in summer, and finally evolved into a strong El Niño event.

Although the unstable coupled ocean–atmosphere system was also formed during the previous fall and winter in 1990 and 2014, the strength of the preceding instability was much weaker compared with that in 1997, and thus the warming in the equatorial central-eastern Pacific was limited in the subsequent months. Moreover, the weak WWB in the spring of 1990 and 2014 led to only weak warming over the ECP, which failed to support the development of positive feedback between WWBs and SSTAs. Since the expected unstable air–sea coupled wave was absent in the spring of 1990 and 2014, the warming over the equatorial central-eastern Pacific was much weaker in spring. Therefore, the zonal SST gradient along the equator in spring 1990 and 2014 decreased slightly

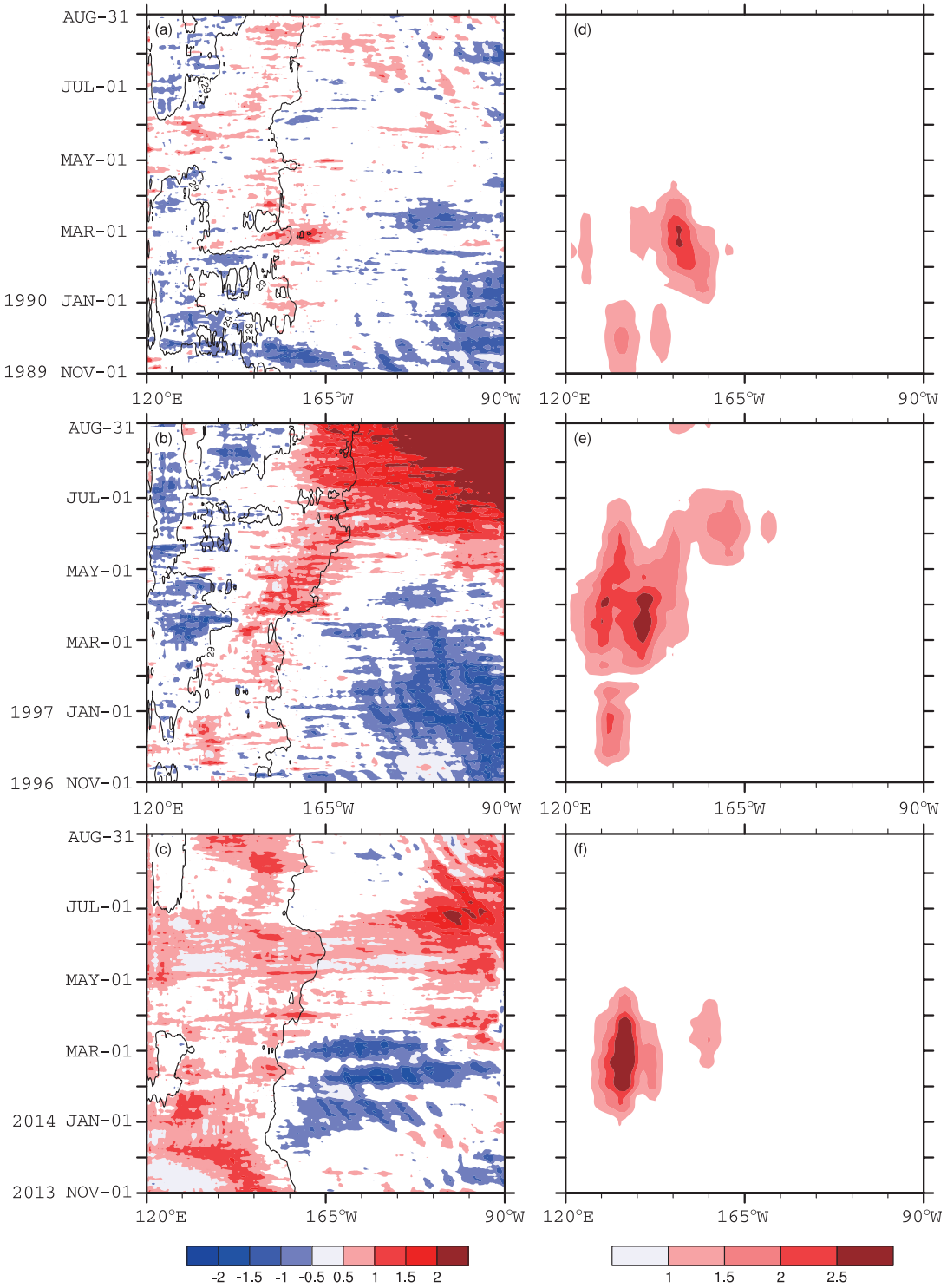

Fig. 4. Time–longitude cross sections of equatorial (5°S–5°N) SSTAs (shading, K) for the periods of (a) 1 November 1989 to 31 August 1990, (b) 1 November 1996 to 31 August 1997, and (c) 1 November 2013 to 31 August 2014. The contour indicates the position of the 29°C isotherm. (d–f) As in (a–c) but for the amplitude of MJO-related WWBs in the equatorial (5°S–5°N) regions (shading, $m^2\ s^{-2}$). See text in section 3.2.1 for the definition of the amplitude of MJO-related WWBs.

and failed to cause a stable negative phase of Southern Oscillation; thus, no positive Bjerknes feedback had established in spring. Therefore, after the instability of the tropical Pacific air–sea coupled system had been removed in late spring, the warming over the equatorial central-eastern Pacific stalled in the summer of 1990 and even decayed in the summer of 2014.

In summary, the strong preceding instability of the tropical Pacific ocean–atmosphere coupled system, as a precondi-

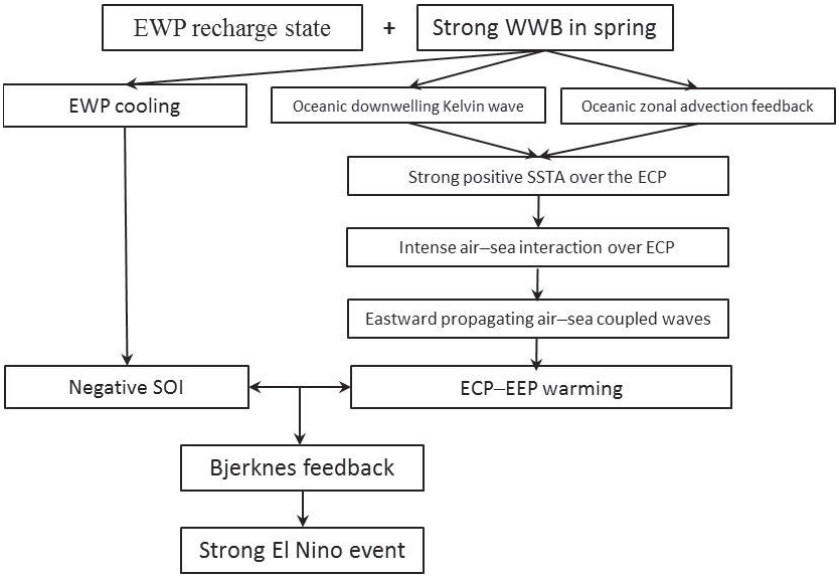

Fig. 5. Schematic diagram showing the key physical processes responsible for a strong El Niño event.

tion, and a strong spring WWB, as a trigger, are two dominant factors responsible for a strong El Niño event. Figure 5 is a schematic diagram illustrating how these two factors lead to a strong El Niño event. For the 2014 event, due to the weak preceding instability and weak WWB in March, the warming in the equatorial central-eastern Pacific suspended in summer. As the weak instability of the ocean–atmosphere coupled system had already been consumed by WWB-induced oceanic waves in spring, and there was no WWB sequence in the summer of 2014, the expected strong El Niño event, like the 1997 super El Niño, was unlikely to occur in the following months of 2014.

It should be noted that, in the present study, we mainly attributed the evolution of the UOHC anomalies to the WWB-associated oceanic waves, as well as the heat transport. However, positive anomalies were still observed in the upper layers of the ECP in August 1990 and August 2014 without WWBs, implying the influence of oceanic internal dynamics on the UOHC anomalies. Moreover, we shall continue to investigate the evolution of UOHC anomalies and SSTAs in the tropical Pacific for the period from fall to winter in 1990 and 2014, thereby improving our understanding of why the El Niño event aborted in 1990 and a weak El Niño event occurred in fall 2014.

Acknowledgements. This research was jointly supported by the National Basic Research Program of China (Grant Nos. 2014CB953902, 2011CB403505, and 2012CB417203), the Priority Research Program of the Chinese Academy of Sciences (Grant Nos. XDA11010402 and XDA01020302), and the National Natural Science Foundation of China (Grant Nos. 41175059 and 41375087).

REFERENCES

Australian Government Bureau of Meteorology, 2014: El Niño remains on hold. [Available online at http://wdev.bom.gov.au/climate/enso/#tabs=Overview.]

Behringer, D., and Y. Xue, 2004: Evaluation of the global ocean data assimilation system at NCEP: The Pacific Ocean. *Eighth Symposium on Integrated Observing and Assimilation Systems for Atmosphere, Oceans, and Land Surface, AMS 84th Annual Meeting*, Washington State Convention and Trade Center, Seattle, Washington, 11–15.

Bergman, J. W., H. H. Hendon, and K. M. Weickmann, 2001: Intraseasonal air-sea interactions at the onset of El Niño. *J. Climate*, **14**, 1702–1719.

Bjerknes, J., 1969: Atmospheric teleconnections from the equatorial pacific. *Mon. Wea. Rev.*, **97**, 163–172.

Chiodi, A. M., D. E. Harrison, and G. A. Vecchi, 2014: Subseasonal atmospheric variability and El Niño waveguide warming: Observed effects of the Madden-Julian Oscillation and westerly wind events. *J. Climate*, **27**, 3619–3642.

Clement, A. C., R. Seager, M. A. Cane, and S. E. Zebiak, 1996: An ocean dynamical thermostat. *J. Climate*, **9**, 2190–2196.

Cronin, M. F., and M. J. McPhaden, 1997: The upper ocean heat balance in the western equatorial Pacific warm pool during September–December 1992. *J. Geophys. Res.*, **102**, 8533–8553.

Fasullo, J., and P. J. Webster, 2000: Atmospheric and surface variations during westerly wind bursts in the tropical western Pacific. *Quart. J. Roy. Meteor. Soc.*, **126**, 899–924.

Fedorov, A. V., S. N. Hu, M. Lengaigne, and E. Guilyardi, 2015: The impact of westerly wind bursts and ocean initial state on the development, and diversity of El Niño events. *Climate Dyn.*, **44**, 1381–1401.

Gill, A. E., 1980: Some simple solutions for heat-induced tropical circulation. *Quart. J. Roy. Meteor. Soc.*, **106**, 447–462.

Hendon, H. H., and M. L. Salby, 1996: Planetary-scale circulations forced by intraseasonal variations of observed convection. *J. Atmos. Sci.*, **53**, 1751–1760.

Hendon, H. H., and J. Glick, 1997: Intraseasonal air-sea interaction in the tropical Indian and Pacific Oceans. *J. Climate*, **10**, 647–661.

Jin, F.-F., 1997: An equatorial ocean recharge paradigm for ENSO. Part I: Conceptual model. *J. Atmos. Sci.*, **54**, 811–829.

Jones, C., D. E. Waliser, and C. Gautier, 1998: The influence of the Madden-Julian Oscillation on ocean surface heat fluxes and sea surface temperature. *J. Climate*, **11**, 1057–1072.

Kalnay, E., and Coauthors, 1996: The NCEP/NCAR 40-year reanalysis project. *Bull. Amer. Meteor. Soc.*, **77**, 437–471.

Kiladis, G. N., G. A. Meehl, and K. M. Weickmann, 1994: Large-scale circulation associated with westerly wind bursts and deep convection over the western equatorial Pacific. *J. Geophys. Res.*, **99**, 18 527–18 544.

Lai, A. W.-C., M. Herzog, and H.-F. Graf, 2015: Two key parameters for the El Niño continuum: Zonal wind anomalies and western Pacific subsurface potential temperature. *Climate Dyn.*, doi: 10.1007/s00382-015-2550-0.

Lau, K. M., and P. H. Chan, 1986: The 40–50 day oscillation and the El Niño/Southern Oscillation: A new perspective. *Bull. Amer. Meteor. Soc.*, **67**, 533–534.

Lau, K.-M., and C.-H. Sui, 1997: Mechanisms of short-term sea surface temperature regulation: Observations during TOGA COARE. *J. Climate*, **10**, 465–472.

Lengaigne, M., J.-P. Boulanger, C. Menkes, G. Madec, P. Delecluse, E. Guilyardi, and J. Slingo, 2003: The March 1997 westerly wind event and the onset of the 1997/98 El Niño: Understanding the role of the atmospheric response. *J. Climate*, **16**, 3330–3343.

Madden, R. A., and P. R. Julian, 1971: Detection of a 40–50 Day Oscillation in the zonal wind in the tropical Pacific. *J. Atmos. Sci.*, **28**, 702–708.

Madden, R. A., and P. R. Julian, 1972: Description of global-scale circulation cells in the tropics with a 40–50 day period. *J. Atmos. Sci.*, **29**, 1109–1123.

Mao, J., and G. Wu, 2007: Interannual variability in the onset of the summer monsoon over the Eastern Bay of Bengal. *Theor. Appl. Climatol.*, **89**, 155–170.

Matsumo, T., 1966: Quasi-geostrophic motions in the equatorial area. *J. Meteor. Soc. Japan.*, **44**, 25–43.

McPhaden, M. J., 1999: Genesis and evolution of the 1997–98 El Niño. *Science*, **283**, 950–954.

Menkes, C. E., M. Lengaigne, J. Vialard, M. Puy, P. Marchesiello, S. Cravatte, and G. Cambon, 2014: About the role of westerly wind events in the possible development of an El Niño in 2014. *Geophys. Res. Lett.*, **41**, 6476–6483.

National Aeronautics and Space Administration, 2014: Is El Niño developing? [Available online at http://earthobservatory.nasa.gov/IOTD/view.php?id=83653]

Philander, S. G. H., 1985: El Niño and La Niña. *J. Atmos. Sci.*, **42**, 2652–2662.

Reynolds, R. W., T. M. Smith, C. Y. Liu, D. B. Chelton, K. S. Casey, and M. G. Schlax, 2007: Daily high-resolution-blended analyses for sea surface temperature. *J. Climate*, **20**, 5473–5496.

Sun, D.-Z., 2003: A possible effect of an increase in the warm-pool SST on the magnitude of El Niño warming. *J. Climate*, **16**, 185–205.

Sun, D.-Z., and Z. Y. Liu, 1996: Dynamic ocean-atmosphere coupling: A thermostat for the tropics. *Science*, **272**, 1148–1150.

Sun, J. Z., T. Li, and R. H. Zhang, 2014: The initiation and developing mechanisms of central Pacific El Niños. *J. Climate*, **27**, 4473–4485.

Sun, X. G., and X. Q. Yang, 2007: Numerical simulations of the interannual climate responses of East Asia to an El Niño event. *Acta. Oceanologica Sinica*, **29**, 21–30.

Taylor, K. E., 2001: Summarizing multiple aspects of model performance in a single diagram. *J. Geophys. Res.*, **106**, 7183–7192.

Tollefson, J., 2014: El Niño tests forecasters. *Nature*, **508**, 20–21.

Toyoda, T., S. Masuda, N. Sugiura, T. Mochizuki, H. Igarashi, M. Kamachi, Y. Ishikawa, and T. Awaji, 2009: A possible role for unstable coupled waves affected by resonance between Kelvin waves and seasonal warming in the development of the strong 1997-1998 El Niño. *Deep-Sea Res.*, **56**, 495–512.

Vecchi, G. A., and D. E. Harrison, 2000: Tropical Pacific sea surface temperature anomalies, El Niño, and equatorial westerly wind events. *J. Climate*, **13**, 1814–1830.

Wang, B., R. G. Wu, and X. H. Fu, 2000: Pacific-East Asian teleconnection: How does ENSO affect East Asian climate? *J. Climate*, **13**, 1517–1536.

Wang, H. J., 2000: The interannual variability of East Asian monsoon and its relationship with SST in a coupled Atmosphere-Ocean-Land climate model. *Adv. Atmos. Sci.*, **17**, 31–47.

Webster, P. J., V. O. Magaña, T. N. Palmer, J. Shukla, R. A. Tomas, M. Yanai, and T. Yasunari, 1998: Monsoons: Processes, predictability, and the prospects for prediction. *J. Geophys. Res.*, **103**, 14 451–14 510.

Wyrtki, K., 1975: El Niño-The dynamic response of the equatorial Pacific ocean atmospheric forcing. *J. Phys. Oceanogr.*, **5**, 572–584.

Wyrtki, K., 1985: Water displacements in the Pacific and the genesis of El Niño cycles. *J. Geophys. Res.*, **90**, 7129–7132.

Xie, S.-P., A. Kubokawa, and K. Hanawa, 1993: Evaporation-wind feedback and the organizing of tropaical convection on the planetary scale. Part I: Quasi-linear instability. *J. Atmos. Sci.*, **50**, 3873–3883.

Xue, Y., and Coauthors, 2012: A comparative analysis of upper-ocean heat content variability from an ensemble of operational ocean reanalyses. *J. Climate*, **25**, 6905–6929.

Yang, S., 1996: ENSO-snow-monsoon associations and seasonal-interannual predictions. *Int. J. Climatol.*, **16**, 125–134.

Zastrow, M., 2014: Stalled El Niño poised to resurge. *Nature*, **513**, 15.

Zhang, C. D., and J. Gottschalck, 2002: SST anomalies of ENSO and the Madden-Julian Oscillation in the equatorial Pacific. *J. Climate*, **15**, 2429–2445.

Zheng, F., J. Zhu, H. Wang, and R.-H. Zhang, 2009: Ensemble hindcasts of ENSO events over the past 120 years using a large number of ensembles. *Adv. Atmos. Sci.*, **26**, 359–372, doi: 10.1007/s00376-009-0359-7.